COMPARISON OF WAVELET TRANSFORM AND CHOI-WILLIAMS DISTRIBUTION TO DETERMINE GROUP VELOCITIES FOR DIFFERENT ACOUSTIC EMISSION SENSORS [#][*]

M. A. HAMSTAD

University of Denver, Department of Mechanical and Materials Engineering, Denver, CO 80208
and National Institute of Standards and Technology, Boulder, CO 80305, USA

Abstract

Acoustic emission (AE) sources in a plate generate dispersive Lamb waves. In this research, pencil lead breaks (PLBs) were made on an edge of a 3.1 mm thick aluminum alloy plate to generate such AE waves. The PLBs were made near the plate mid-plane and near the bottom of the edge. The waves were sensed by pairs of AE sensors (both resonant or both non-resonant wideband). Each sensor of each pair was located at a different distance from the plate edge PLB position. The signals from the different sensors and source positions were analyzed and contrasted. The recorded signals were processed by a wavelet transform (WT), and the group velocity curves for the appropriate Lamb modes were superimposed to clearly identify the modes in the signal. The threshold-independent mode arrival times at specific intense signal frequencies were determined by the time of the peak WT magnitude at the intense frequency. Since the two sensors were located at different known distances from the PLB position, an experimental group velocity was calculated based on the difference in arrival times and the difference in distance. This velocity was then compared to the theoretical group velocity for the relevant mode and frequency. In addition, an alternate frequency/time analysis method was used. This was the Choi-Williams distribution (CWD). The same procedures used for the WT results were followed for the CWD distribution. In addition the experimental results were compared to finite element calculated results for plate-edge monopoles both near the mid-plane and near the top plate edge. Group velocities within 6.5 % of the theoretical values were obtained with all the sensor types when certain intense resonant frequencies were ignored for two of the three resonant sensor types.

Introduction

The author and his co-workers have published a number of papers on the analysis of finite-element modeled (FEM) acoustic emission (AE) signals in a 4.7 mm thick aluminum plate [1- 6]. One focus of this work has been to demonstrate the use of a wavelet transform (WT) to obtain accurate and threshold-independent arrival times from the peak WT magnitude of certain intense frequencies of the Lamb modes. Since these arrival times were associated with specific known group velocities, very accurate source locations could be calculated for the dispersive AE waves

---

[#] Contribution of the U.S. National Institute of Standards and Technology; not subject to copyright in the United States
[*] Trade and company names are included only for complete scientific/technical description; endorsement is neither intended nor implied.

even in the presence of significant electronic preamplifier noise [6]. This result was due to the fact that the WT spreads out the noise in frequency, while the arrival of a mode in an AE signal concentrates the signal energy at specific frequencies and specific times. In addition, since WT-based arrival times are obtained from regions of the AE signal that have significant amplitude, the above approach is also much more robust in the presence of preamplifier noise than AE analysis techniques that seek to obtain the arrival time from the very first arrival of an AE signal. This result is due to the fact that the first arrival region of an AE signal is often considerably lower in amplitude than the peak region of the signal. Thus, the very first arrival may be "lost" in the noise.

Due to the small spatial resolution of the FEM results (typically a 0.3 mm cell size), the WT-based arrival times were in essence obtained from the signal from a perfectly flat-with-frequency point-contact "pseudo" displacement sensor. Thus, a question remains with respect to the above research. What is the accuracy of arrival times obtained in a similar fashion from the signals from real AE sensors?

The purpose of the research reported here was to examine with signals from real AE sensors whether experimentally obtained mode arrival times from pencil lead break (PLB) generated waves accurately corresponded to theoretical group velocities in a thin aluminum plate. These experiments were done using a variety of AE sensor types, and the arrival times were determined from frequency/time analysis, as was done with the FEM-generated results. The sensors included both wideband (with response approximately flat with frequency over certain frequency ranges) and resonant sensors (this characterization of the sensors was based on information available from sensor suppliers). Both a WT and the Choi-Williams distribution (CWD) were compared relative to their use for determination of accurate mode arrival times as measured by the closeness of the experimental group velocities to theory. These comparisons were made from the arrival times of the more intense modal regions in the frequency/time magnitude results.

Experiment

Previous finite element modeled results as well as experimental results demonstrated that PLBs applied to the edge of a plate generated AE waves that were much more similar to the AE from modeled results from interior buried dipole AE sources than PLBs applied to the plate top or bottom surface [7,8]. Hence, PLBs (0.3 mm diameter, 2H hardness, length of about 2 mm) were applied to the edge of an aluminum alloy plate having a thickness of 3.1 mm. Two sensors of each type were mounted at a time on the upper plate surface by use of vacuum grease as the couplant. They were mounted on a line perpendicular to the plate-edge PLB position (located at the midpoint along the long edge of the plate). One sensor was mounted at 127 mm (5 in.) from the edge, and the other at 305 mm (12 in.). Based on the results of previous modeling that showed the modal distribution of energy in an AE signal strongly depended on the source depth in a plate [1], the pencil lead was broken in contact with the plate edge near the mid-plane and also near the bottom of the edge. A third AE sensor located on the plate top surface near the PLB point was used to provide a consistent trigger signal for a 12-bit transient digital recorder. A passive four-pole Butterworth filter was used to high-pass the signals at 50 kHz before the signals were recorded with a time step of 0.1 μs. A total of six different models of AE sensors were used, including two commercially available wideband sensors (designated WB #1 and WB #2) and three commercially available resonant sensors (designated Res #1, Res #2 and Res #3). In addition, a high sensitivity wideband sensor developed at NIST Boulder was used (designated FHWA) [9, 10]. Some information about the sensors is shown in Table 1. No special purchase

Table 1 Listing of sensors used.

Sensor names	Expected response character	Freq. [kHz] of peak response
FHWA	Wideband	Not applicable
WB #1	Wideband	Not applicable
WB #2	Wideband	Not applicable
Res #1	Resonant	125
Res #2	Resonant	500
Res #3	Resonant	150

of sensors was made; instead available sensors from other projects were used. Appropriate pre-amplifiers and preamplifier gains were used with each sensor. In all cases the high-pass frequency of the preamplifiers was either 1 kHz or 5 kHz, and the low-pass frequency was at least 1 MHz. A total of at least three PLBs was made for each source position for each set of sensors to make sure that representative results were obtained. In the analysis, only the representative signals from one PLB (per source position) were used for each set of sensors. The transverse dimensions of the plate (1220 mm by 1525 mm) were large enough to preclude reflections from the plate edges arriving during the duration of the waves propagating directly from the PLB position to the sensors.

In addition, finite element modeled results were also obtained for a 3.1 mm thick aluminum plate. These results were "converted" from existing results for a 4.7 mm thick aluminum plate by use of a technique previously demonstrated [11]. Because the "converted" 3.1 mm thick results were generated from the existing results for a different plate thickness and propagation distance, the in-plane monopole source depths (below the top surface of the plate) and the propagation distance were directly determined by the "conversion" process applied to the original data. Thus, the propagation distance to the "pseudo" sensor position was 120 mm from the monopole source applied to the plate edge. In addition, the two source depths were 0.52 mm (near the plate top edge) and 1.35 mm (near the plate mid-plane) below the top plate surface. After the conversion process was applied to the unfiltered FEM data, the signal that represented the out-of-plane top surface displacement versus time was digitally filtered with a four-pole 50 kHz high-pass Butterworth filter and then resampled in time from 29.6 ns to 0.1 µs per point. The resultant data corresponded to the sampling interval of the experimental data. The domain of the plate for the finite element modeled (FEM) data was smaller in size (530 mm on the source side by 330 mm in the propagation direction) than the experimental plate. The plate was still of sufficient size that edge reflections did not occur during the full arrival of the signal that propagated directly from the source to the "pseudo" sensor position.

Group Velocity Curves for a Thin Aluminum Plate and Frequency/Time Analysis Procedures

Group velocity curves [12] of the fundamental symmetric and the first two antisymmetric Lamb modes for the 3.1 mm thick plate are shown in Fig. 1. Additional group velocity modes were not considered because their frequencies were beyond those normally used in AE for the current plate thickness. WTs [12] of the signals from the PLBs and FEM results were calculated. Group velocity curves were superimposed on the WT results by use of the known propagation distances. To correctly superimpose the group velocity curves (after the effect of propagation distance was accounted for), the curves were offset in time to match (by eye) the WT experimental results for the FHWA sensor. Then this same time offset was used for all the other
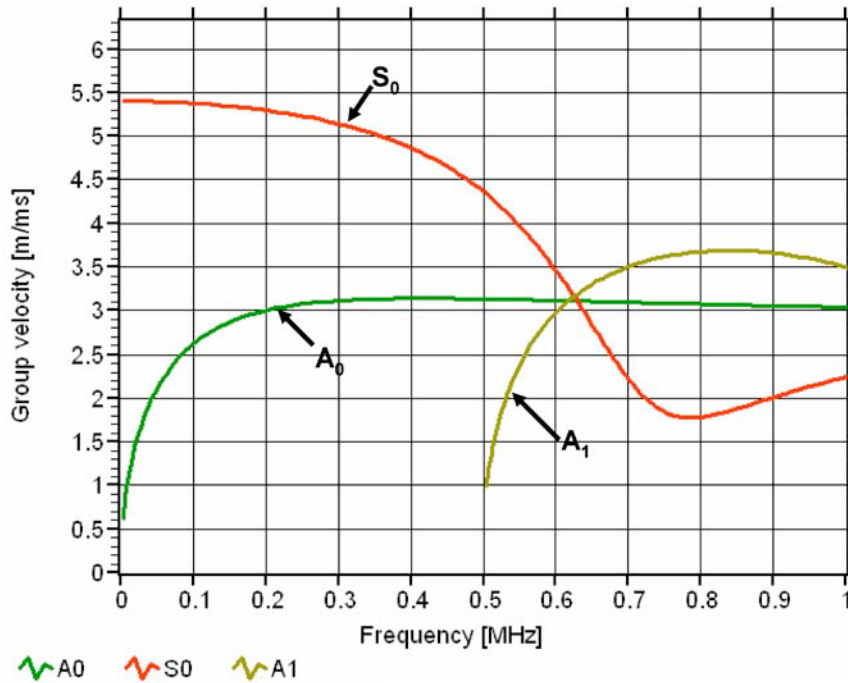
Fig. 1. Relevant group velocities vs. frequency for an aluminum plate of 3.1 mm thickness [12].

sensor results. This time adjustment was not necessary for the FEM results, because the displacement versus time data started at the time of the AE source initiation. The key parameters chosen for the WT calculation were a frequency resolution of 3 kHz (frequency band) and a wavelet size of 600 samples. In addition, a feature of the WT software was used to determine the frequencies, arrival times (at the peak magnitude of the frequency band) and the peak magnitude of the more intense mode arrivals.

An alternate frequency/time analysis was also applied to each experimental signal and to the FEM results. This approach was the CWD. This computation was made using the LabVIEW implementation (Easy CWD) [13]. Other than the default parameters, the following settings were used: (i) 2048 frequency bins, (ii) time resolution of 0.1 µs, (iii) analytic signal and (iv) $\alpha = 0.1$ (this parameter controls the balance between resolution and cross-term interference). The CWD implementation did not allow for the superposition of the group velocity curves, but it was easy to pick out the modes by eye by use of the insight from the WT results for the same signals. Again the frequency, arrival times (at the peak of the frequency band) and the peak magnitude of the more intense mode arrivals were obtained from the CWD results by use of custom additions to the LabVIEW programming.

The frequencies of the intense mode arrivals were reported as the frequency at the high end of the WT and CWD frequency bands. Because the CWD bands were 2.44 kHz wide, the reported frequency was the largest number without decimal values in each band.

Typical Time Domain Results for Signals from Experimental PLBs and the FEM Data

Because the spread in time between the modes increased as the propagation distance increased, the signals at the farther distance (305 mm) were initially selected for more detailed examination. Thus, mode identification was enhanced. For an edge in-plane PLB near the midplane of the plate, Fig. 2 illustrates typical experimental time domains of the signals from all
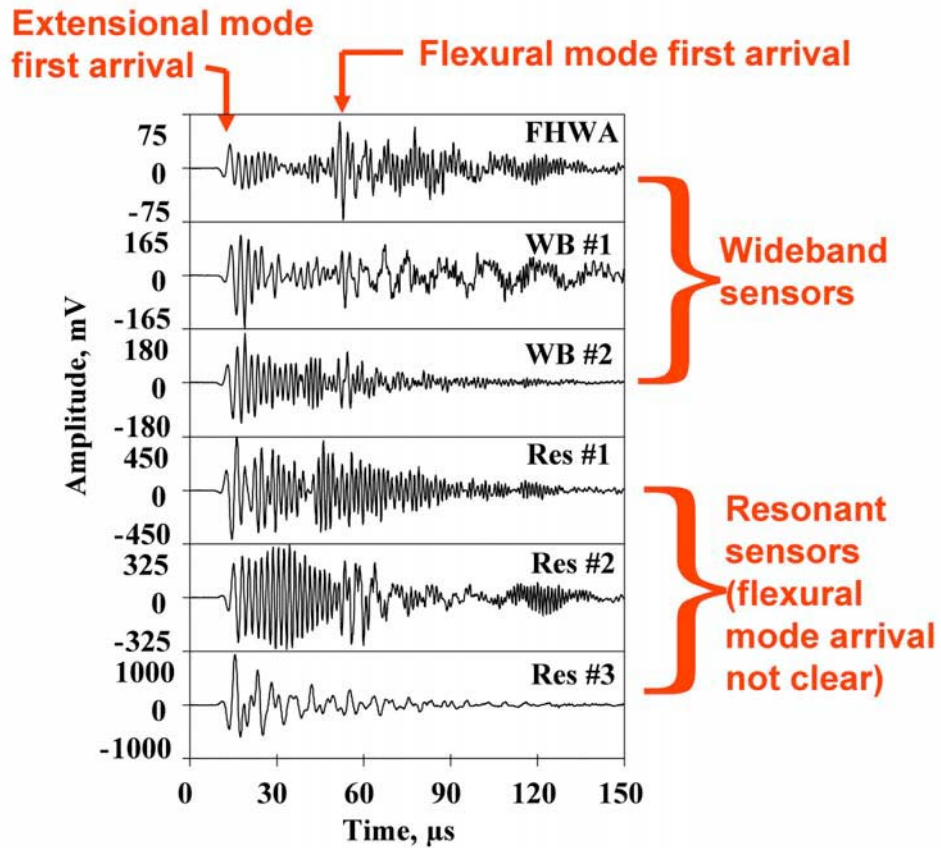
43

Fig. 2. Time domains for the different sensors at 305 mm propagation distance from PLB near the mid-plane of plate.
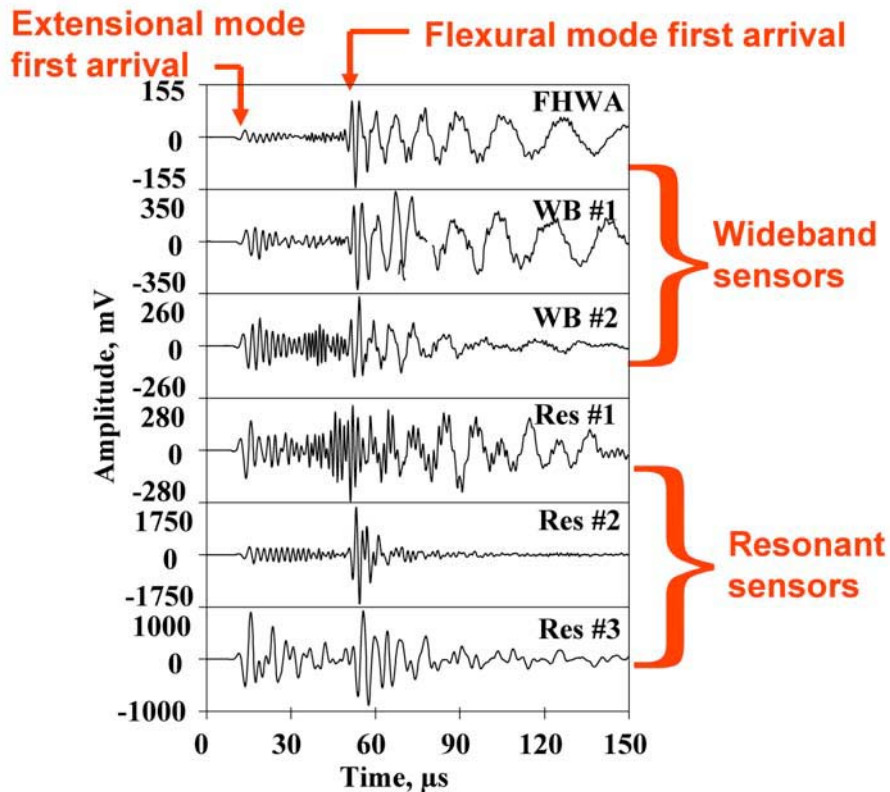

Fig. 3. Time domains for the different sensors at 305 mm propagation distance from PLB near the bottom edge of plate.

the sensor types. Figure 3 shows the typical time domain results for an in-plane edge PLB near the bottom of the plate.

Figure 2 demonstrates that for nominally the same displacement wave passing beneath the sensors, there was a wide variety of waveforms from the different sensors for the near mid-plane PLB. Only the wideband FHWA and WB #1 sensor signals were reasonably similar. As expected from the group velocity curves, the S_0 (extensional) mode first arrival was clearly observed at the beginning of all the signals. From the wideband sensor signals, the first arrival of the A_0 (flexural) mode can also be identified by eye, as indicated by the arrow in Fig. 2. In contrast, the first arrival of the flexural mode cannot be easily identified in the resonant sensor signals. Close examination by use of an expanded time scale of the signal from the Res #2 sensor does show the first arrival of the A_0 mode, but it was a little later than with the wideband sensors.

For the PLB source near the bottom edge, Fig. 3 shows the first arrival of the extensional mode for all the sensor signals. Also, with the exception of the Res #1 sensor, the first arrival region of the flexural mode can be identified by eye, as indicated by the arrow in Fig. 3. For this source position, the time domain signals were still quite different from each other, but they were more similar to each other than for the near mid-plane source. The signals from all three wideband sensors were the most like each other for the near bottom edge source.
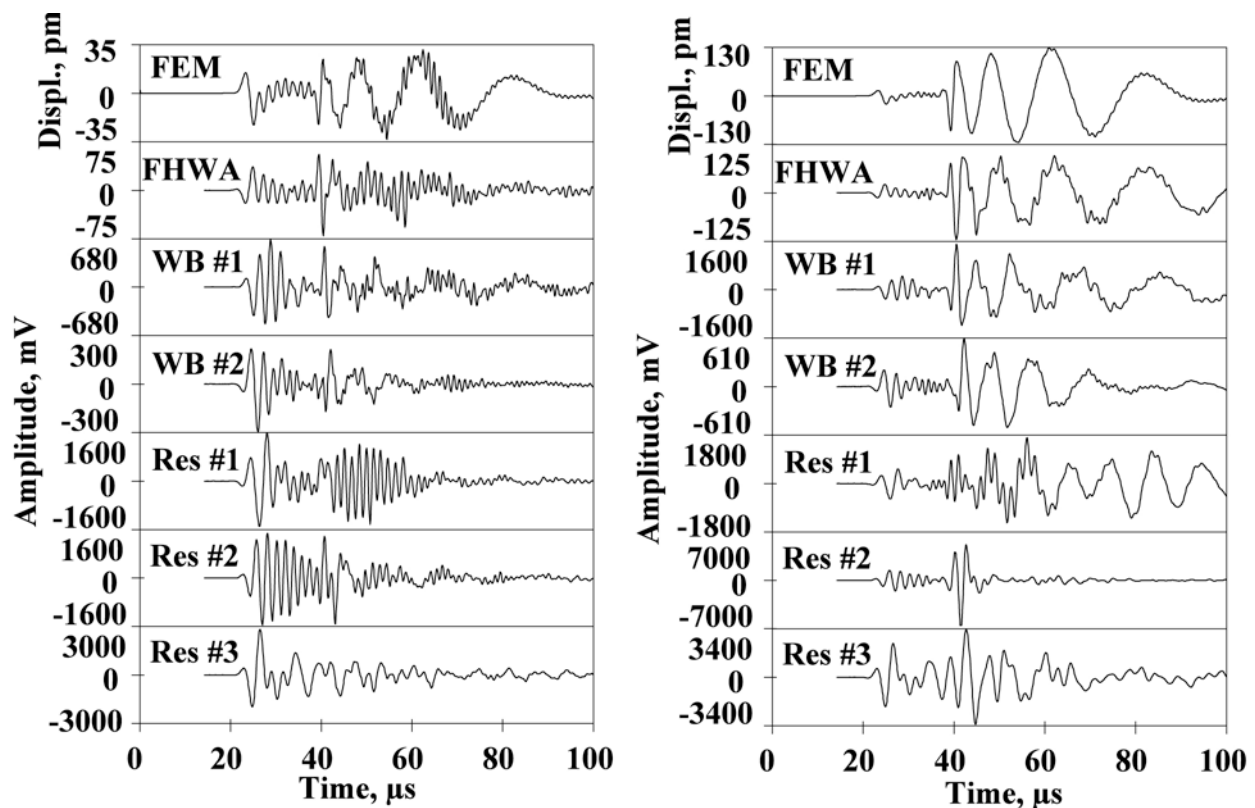

Fig. 4. FEM displacement at 120 mm propagation distance and sensor signals at 127 mm for in-plane source. Left column source near mid-plane and right column source near a plate surface.

It is of interest to compare the PLB results with the FEM results. Figure 4 shows the FEM out-of-plane displacement versus time for the in-plane edge monopole source located at two depths. These results are shown as the top waveforms in part (a) at 1.35 mm depth (near the mid-plane) and in part (b) at 0.52 mm depth (near the top edge). Figure 4 also shows the PLB waveforms for the different sensors at the 127 mm propagation distance. Although the

propagation distance of the FEM result was a little less at 120 mm, it is clear that both the extensional and flexural mode signals show clear first arrival regions in the FEM signals, while the PLB signals in general show mode arrival characteristics similar to those discussed above for the larger propagation distance. In addition, it is worthwhile to note that the wideband sensor signals were much closer to those from the FEM computation. The resonant sensor signals were not nearly as close to the FEM-based signals. In closing this paragraph, we point out that the only significant difference between a source near the top edge (FEM data) and one near the bottom edge (PLB data) is a change in phase of the anti-symmetric modes.
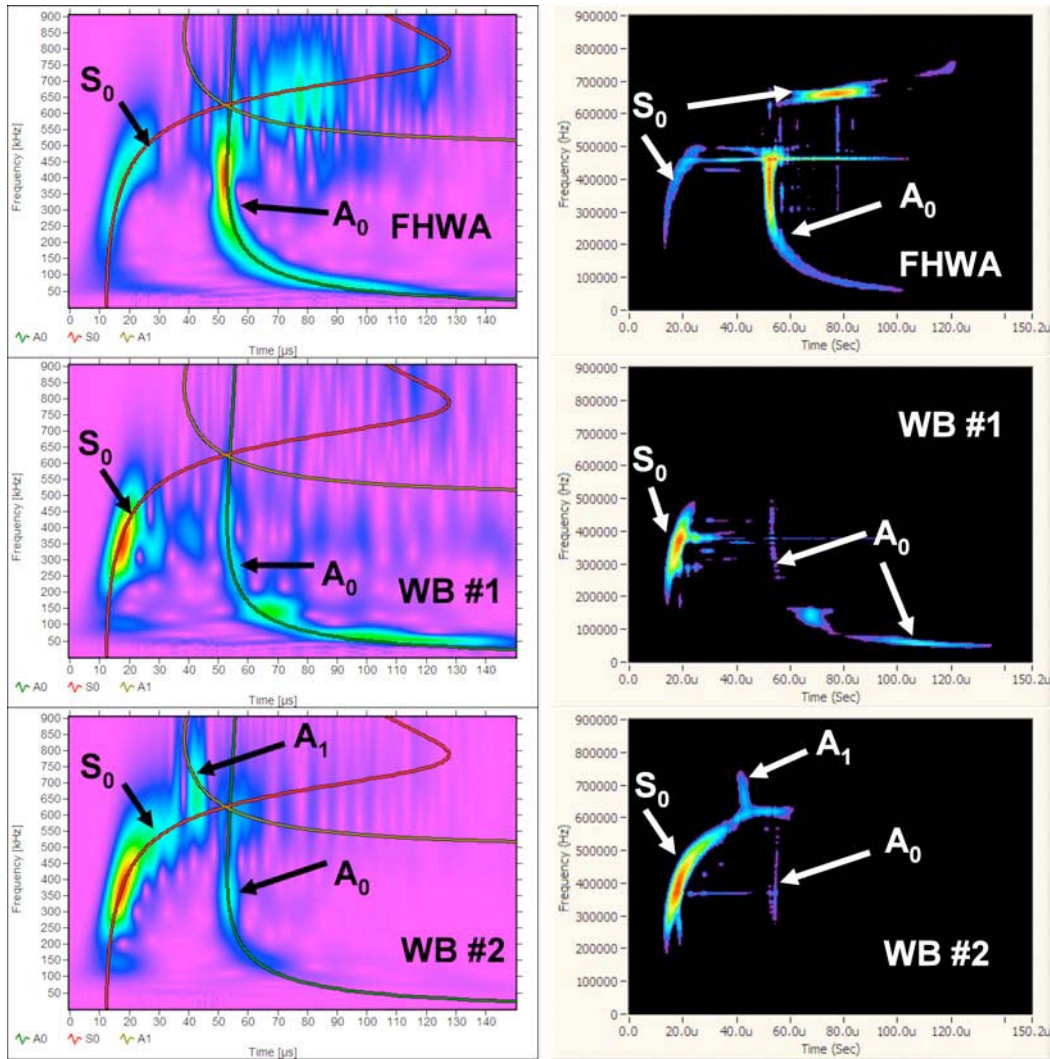

Fig. 5. WT (left column) and CWD (right column) of signals (Fig. 2) resulting from PLB near the mid-plane of the plate sensed by wideband sensors at a propagation distance of 305 mm.

Typical Frequency/Time Results for Signals from Experimental PLBs and the FEM Results

The left columns of Figs. 5 through 8 show the results after the WT was applied to the sensor signals. The A_0 and S_0 modes are labeled in all the figures, and the A_1 mode is labeled in figures where it was relevant. Figures 5 and 7 respectively show the wideband sensor results for the near mid-plane and near bottom edge PLBs. Figures 6 and 8 respectively show the resonant sensor results for the near mid-plane and near bottom edge PLBs. With the help of the group velocity
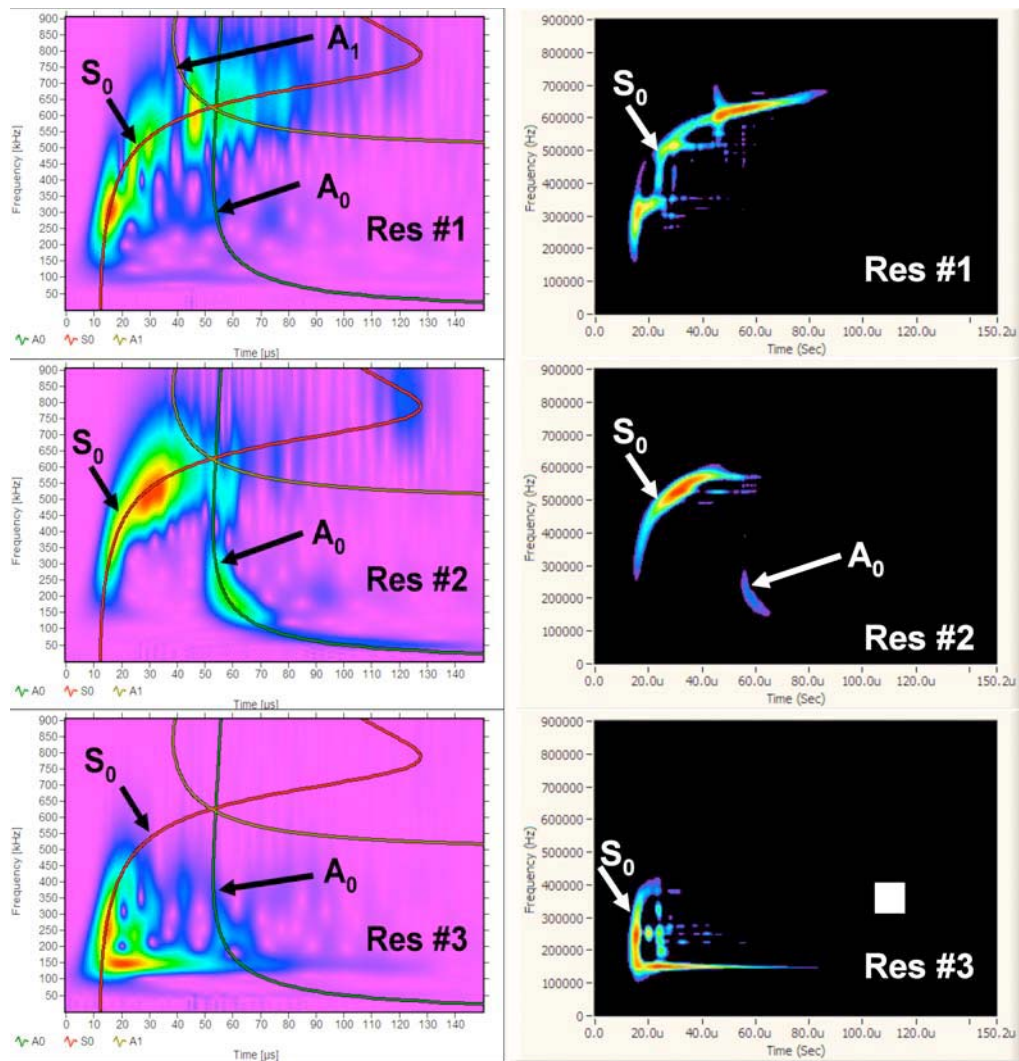
Fig. 6. WT (left column) and CWD (right column) of signals (Fig. 2) resulting from PLB near the mid-plane of the plate sensed by resonant sensors at a propagation distance of 305 mm.

curves at the known propagations distances, it was easy to identify the modes that were intense for all the sensors at both source depths. Thus the WT results provide a clearer picture of the modes and their arrivals than do the original amplitude versus time results. This result is particularly the case for the resonant sensors. Of even more importance, the WT results also identified the frequencies within the modes that were most intense for the different sensors at the two different source depths.

Because the waves that the sensors responded to were very similar for each PLB position, the WT results demonstrate significant distinctions between the response characteristics of the different sensors. First, considering the wideband sensor data for the near mid-plane source, the FHWA sensor responded most strongly in the A_0 mode, while the other two wideband sensors responded most strongly in the S_0 mode (see Fig. 5). Second, with these same three wideband sensors for the near bottom edge source, the signals responded most strongly in the A_0 mode. For this source depth, Fig. 7 shows that there were two regions of most intensity in the A_0 mode for the signals from the WB #1 and WB #2 sensors, and only one lower frequency region for the signals from the FHWA sensor.
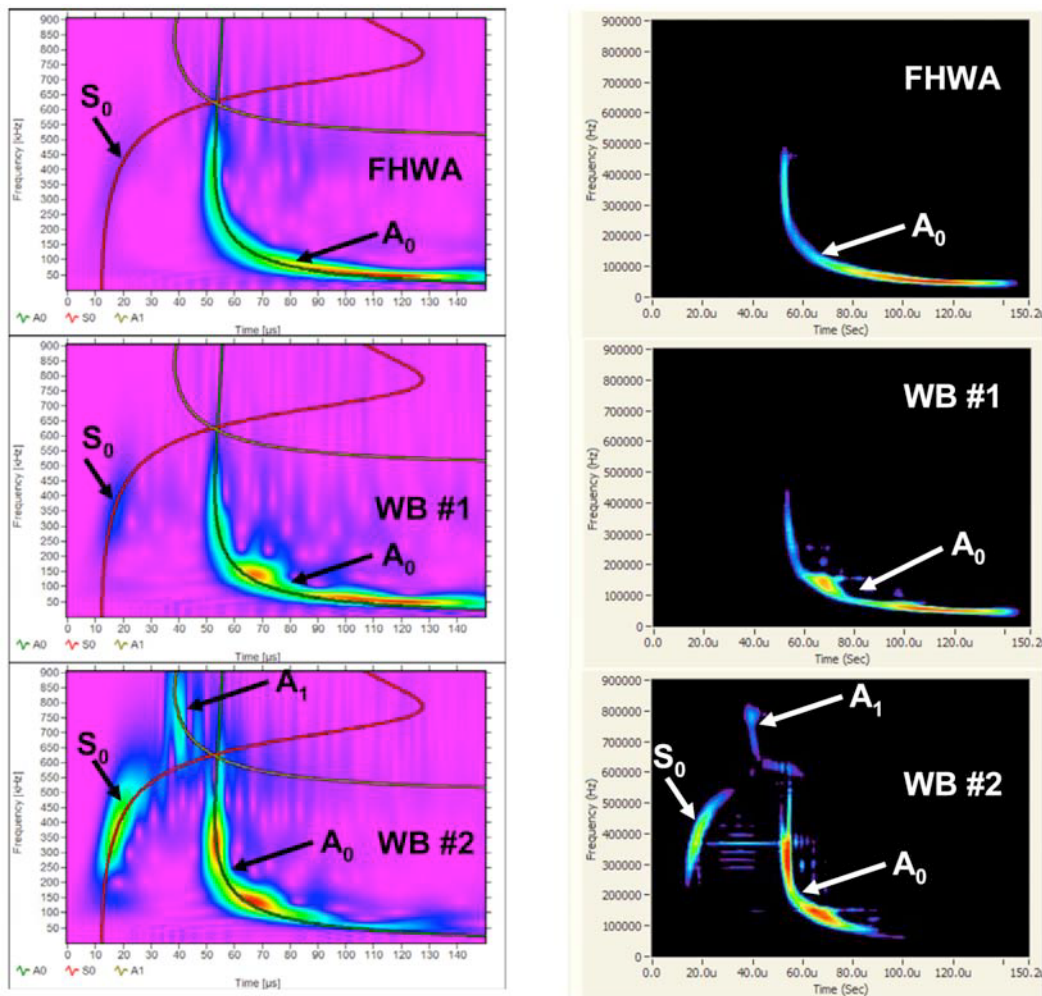
Fig. 7. WT (left column) and CWD (right column) of signals (Fig. 3) resulting from PLB near the bottom edge of the plate sensed by wideband sensors at a propagation distance of 305 mm.

Examination of the resonant sensors WT results shown in Fig. 6 for the near mid-plane source position showed that the S_0 mode was dominant in the signals from each sensor. In addition the figure showed that there was a considerable difference in the dominant frequency within that mode for the different sensors. For the source position near the bottom edge, the A_0 mode dominated for all the resonant sensors, as can be observed in Fig. 8. Again there was a wide range in the most dominant frequency within the mode. When the WT results for the different resonant sensors were examined in more depth, it was found that not only are there different frequencies within the modes more intense than those that were intense for the wideband sensors, but there is evidence that points to resonances within the signals from these sensors. For example for the near mid-plane source, the Res #3 sensor result shows a time-extended high intensity region of the S_0 mode at about 150 kHz (see Fig. 6). This resonance was expected based on the characteristics of this sensor. Another example of such behavior was present in the WT results of the Res #1 sensor signal for the source near the bottom edge. In this case, there was an extended intense region at about 100 kHz, where the intense region starts at the A_0 mode curve and then continues with intensity (as time increases) at this same frequency (see Fig. 8). These examples of resonant behavior were not present in the wideband sensor results. For example in contrast to the Res #1 result, for the same near bottom edge source position, the FHWA sensor's intense region closely follows the A_0 mode curve (see Fig. 7).
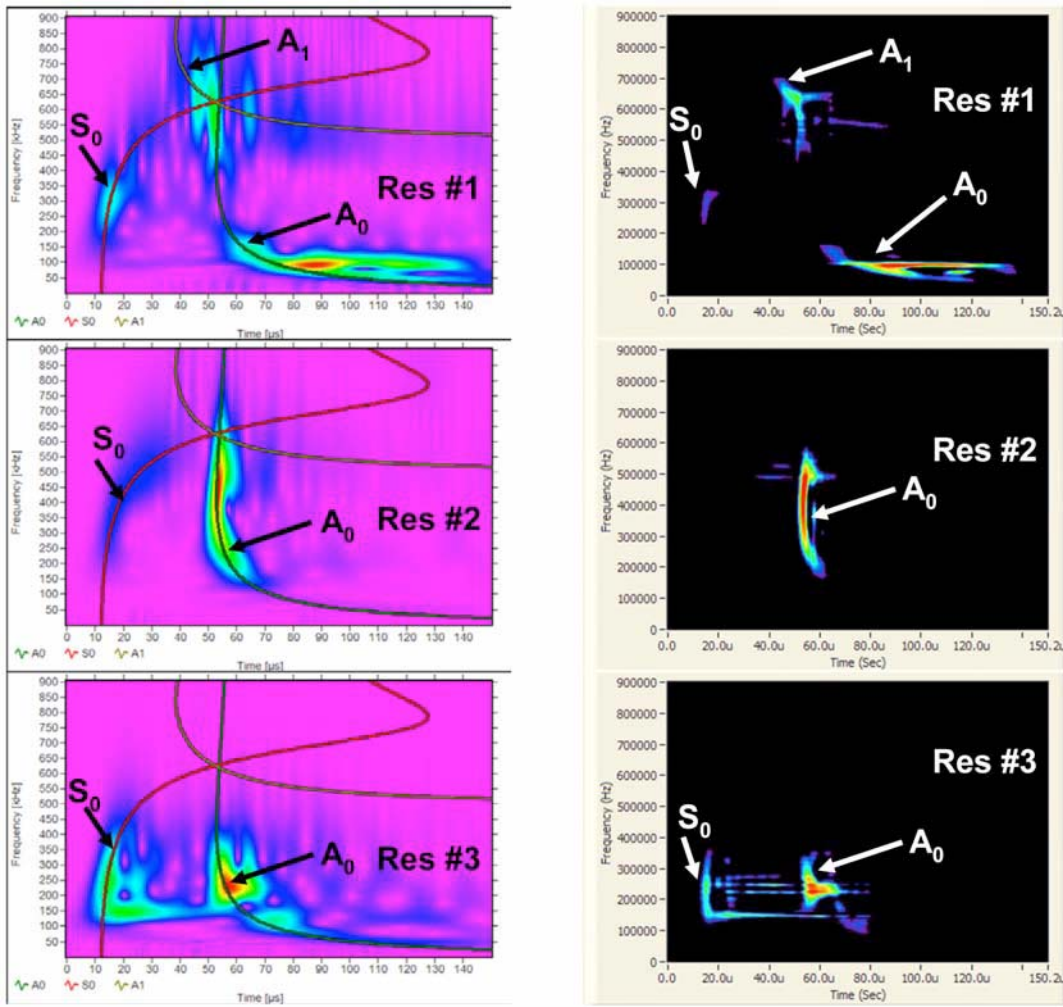
48

Fig. 8. WT (left column) and CWD (right column) of signals (Fig. 3) resulting from PLB near the bottom edge of the plate sensed by resonant sensors at a propagation distance of 305 mm.

Corresponding to the WTs of the signals from the different sensors for the two source positions, the CWD results from the sensor signals are shown in the right columns of Figs. 5 through 8 for the 305 mm propagation distance. Based on the adjacent WT results, the intense modes in the CWD were labeled as shown. The most intense regions for each sensor at each depth were similar to the WT results except for a slight difference in the CWD for the FHWA sensor for the in-plane source. In this case, there is an additional intense region within the S_0 mode at approximately 650 kHz in the CWD result. This region does not show as strongly in the WT result for this signal. Further contrasts between the CWD and the WT results will be discussed later in this paper.

The WT and CWD results were also obtained from the FEM-generated signals at the two depths. Figure 9 shows these results in the left column for the near mid-plane source results and in the right column for the near top surface results. Due to the fact that the FEM results represent those from a perfect wideband sensor, it makes the most sense to compare them with the experimental results from the wideband sensors. In this comparison, there was a significant difference for the near mid-plane result. For the FEM signals, the WT and CWD (respectively Figs. 9(a) and (c)) results show that the most intense region was in the low frequency region (centered around 60 kHz) of the A_0 mode. In the experimental case for the near mid-plane PLB, the most intense region, except for the FHWA sensor, was in the S_0 mode at both propagation distances
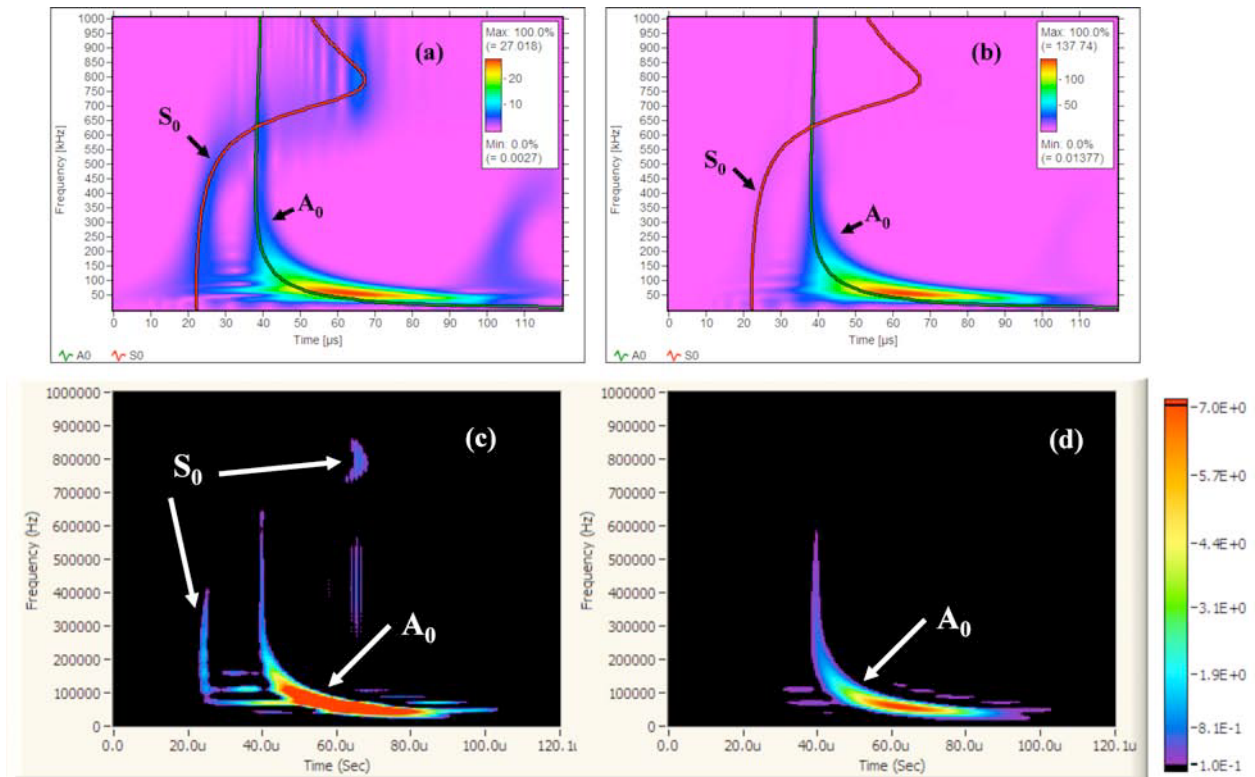
49

Fig. 9. WTs of finite element modeled signals shown in top row of Fig. 4; (a) near mid-plane source and (b) near top edge. CWD for the same two modeled signals; (c) and (d) correspond respectively to the signals resulting in the WTs in (a) and (b).

(results at 127 mm are not shown). For the FHWA sensor the most intense mode was the A_0 mode, but the intense frequency regions were at higher frequencies than with those from the FEM results. Specifically the FHWA signal had two nearly identical magnitude WT peaks at 291 kHz and 513 kHz at the 127 mm distance, and at the 305 mm distance the most intense WT peak was at 405 kHz. For the source position nearer a plate surface, the FEM result (Figs. 9(b) and (d)) was quite similar to the experimental wideband sensor results at both distances (results for the 127 mm distance are not shown) for the FHWA and WB #1 sensors, as shown in Fig. 7 at the 305 mm distance, with the most intense region being in the low frequency region centered around 60 kHz (at the 127 mm distance the results were similar, but are not shown). The WB #2 sensor had its most intense region at a higher frequency of the A_0 mode centered at about 138 kHz in the WT result. This observation indicates the WB #2 sensor has a poorer low frequency response compared to that of the other two wideband sensors.

Group Velocity Results for PLBs near the Mid-plane and Bottom-edge of the Plate

Because, as previously noted, the individual mode/frequency combinations with significant intensity are most easily characterized at the further propagation distance, the WTs and CWDs for the 305 mm propagation distance were used to define the intense mode/frequency combinations (i.e., the regions in the frequency versus time plane where the magnitudes of the WT or CWD were large at mode arrivals) to be used to determine mode arrival times at both propagation distances. It is worth noting that the frequency at the peak within the modes was not exactly the same for the WT and CWD for a particularly intense modal region. The process of determining of arrival times is demonstrated in Fig. 10 for a signal from the FHWA sensor for a near mid-

Table 2 Mode/Frequency combinations and group velocities for PLB near mid-plane.

Sensor	Mode/Frequency [kHz]	Magnitude as a percentage of maximum	Experimental group velocity [mm/µs]	Theory group velocity [mm/µs]	Signed percentage difference in velocity
FHWA	A_0/405	100	3.16	3.14	0.6
	A_0/463	100	3.03	3.14	-3.4
	S_0/627	55	2.78	2.91	-4.7
	S_0/661	93	2.56	2.46	4.1
WB #1	S_0/351	100	5.08	4.99	1.8
	S_0/371	100	4.91	4.93	-0.4
	A_0/141	62	2.80	2.85	-1.7
	A_0/146	36	2.80	2.87	-2.5
	A_0/60	61	2.34	2.26	3.6
	A_0/61	36	2.26	2.30	-1.9
WB #2	S_0/375	100	4.95	4.92	0.7
	S_0/397	100	4.89	4.84	0.9
Res #1	S_0/306	100	5.37	5.12	5.0
	S_0/307	83	5.44	5.11	6.5
	S_0/441	77	4.49	4.63	-3.0
	S_0/517	71	4.32	4.13	4.5
Res #2	S_0/510	100	4.04	4.18	-3.3
	S_0/527	100	4.03	4.05	-0.4
	A_0/195	66	2.99	3.00	-0.5
	A_0/222	22	3.09	3.05	1.8
Res #3	S_0/147	100	5.40	5.35	1.1
	S_0/153	100	5.37	5.34	0.6
	S_0/252	94	5.25	5.22	0.5
	S_0/251	98	5.26	5.22	0.5

plane PLB. This figure shows the signal, the CWD and WT, and the magnitude versus time of both the CWD and the WT coefficients for the 405 kHz frequency band. The time of the maximum magnitude peak was used to define the arrival time of the A_0 mode in this case. Using the differences in the arrival times (since the signals from the two sensors had a common trigger) an experimental group velocity was calculated based on the difference in propagation distance of 178 mm. Table 2 summarizes the more intense mode/frequency combinations and their relative magnitude (from the 305 mm results) at the mode arrival along with the calculated experimental group velocity. The relative magnitude was calculated based on the maximum frequency/time intensity for the whole signal. In addition, the table shows the theoretical group velocities (from the data shown in Fig. 1) and a sign-based percentage difference of the experimental velocity relative to the theoretical one. In the table, there are two lines for each mode/frequency case. The first line gives the WT results, and the second line gives the associated CWD results for each sensor and mode/frequency case. When the local maximum of an intense frequency was near the 50 kHz filter's high-pass frequency, a frequency of 60 kHz was used for the WT and 61 kHz for the CWD. Only the intense mode/frequency combinations that had magnitude maxima for the same mode at both propagation distances at the frequency determined from the 305 mm distance data were considered. Also, the table does not include intense frequencies where the mode could not be clearly indentified.

Following the same procedures used to create Table 2, Table 3 was created for the PLB source near the bottom edge of the plate. In both tables, only the fundamental modes appear.
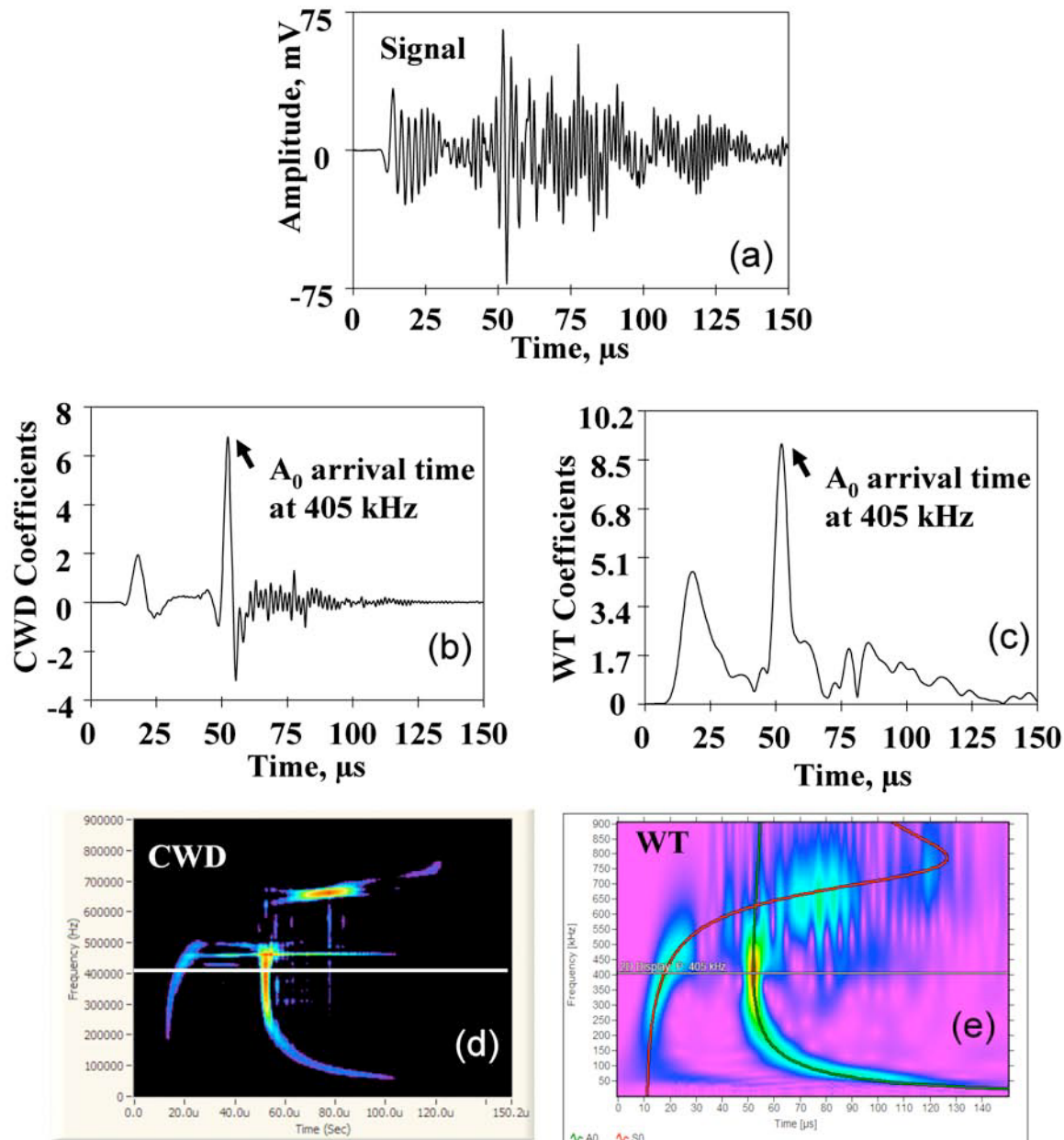
Fig. 10. Illustration of determination of the A_0 mode arrival times for the signal (FHWA sensor for near mid-plane PLB; propagation distance 305 mm) shown in (a). The CWD and WT coefficients at 405 kHz are shown respectively in (b) and (c). The full CWD and WT are shown respectively in (d) and (e) with a line at 405 kHz.

Observations Based on Tables 2 and 3

In spite of the dominance of a particular mode for each of the two source positions, Tables 2 and 3 show that the frequencies that were intense within each mode varied widely over the six different sensors. Interestingly, this was the case even for the wideband sensors (for the near mid-plane source and the S_0 mode, the minimum and maximum intense frequencies were 60 kHz and 661 kHz; for the source near the bottom edge and the A_0 mode these maximum and minimum frequency values were respectively at 60 kHz and 384 kHz). With the resonant sensors, the range of intense S_0 mode frequencies varied from 147 kHz to 527 kHz for the near mid-plane source, and the range of A_0 mode frequencies varied from 93 kHz to 466 kHz for the

near bottom edge source. It seems most likely that these wide variations in the intense frequencies within the modes were due to both the intense mode/frequency combinations in the generated Lamb waves and the details of the different sensor's response sensitivity as a function of frequency. Thus, the observed intense mode frequencies do not in general directly correlate with the sensor resonant frequencies.

Table 3 Mode/Frequency combinations and group velocities for PLB near bottom edge.

Sensor	Mode/Frequency [kHz]	Magnitude as a percentage of maximum	Experimental group velocity [mm/µs]	Theory group velocity [mm/µs]	Signed percentage difference in velocity
FHWA	$A_0/60$	100	2.23	2.26	-1.6
	$A_0/61$	100	2.25	2.30	-2.2
	$A_0/384$	64	3.16	3.14	0.6
	$A_0/346$	45	3.15	3.13	0.6
WB #1	$A_0/60$	100	2.32	2.26	2.4
	$A_0/61$	100	2.27	2.30	-1.3
	$A_0/141$	96	2.80	2.85	-1.7
	$A_0/146$	88	2.78	2.87	-3.1
	$A_0/288$	58	3.09	3.11	-0.7
	$A_0/317$	38	3.11	3.12	-0.5
WB #2	$A_0/138$	100	2.88	2.83	1.6
	$A_0/151$	100	2.87	2.88	-0.2
	$A_0/330$	99	3.21	3.13	2.6
	$A_0/349$	100	3.17	3.13	1.2
Res #1	$A_0/93$	100	3.77	2.59	45
	$A_0/100$	100	3.41	2.64	29
	$S_0/300$	43	5.39	5.14	4.8
	----	----	----	----	----
Res #2	$A_0/441$	100	3.16	3.14	0.9
	$A_0/466$	100	3.16	3.16	0.7
Res #3	$A_0/231$	100	3.08	3.06	0.8
	$A_0/239$	100	3.07	3.07	0.3

Since the time domain signals processed by both the CWD and the WT were identical, it was not surprising that there were related pairs (except for one case) of intense regions as shown in Tables 2 and 3. In the single case in Table 3 for the Res #1 sensor, the CWD did not have the same peak modal location at both propagation distances; hence no result is included in the table in this case. Examination of these pairs shows that generally the CWD gives a higher frequency for the frequency of the intense regions of the modes (ignoring the cases of the arbitrarily selected frequencies of 60 and 61 kHz). This result seems to be consistent with those of the following experiment. Three sine waves of frequencies 60 kHz, 270 kHz and 522 kHz (all with the same amplitude, with a 0.1 µs time step) were superimposed, and then the WT and CWD were applied. For the results shown in Fig. 11, the CWD band magnitudes (that included the sine wave frequencies) expressed as a percentage from low to high frequency were 100, 100 and 67. On the other hand, the WT magnitudes show an increasingly greater reduction at the higher frequencies, since their respective values were 100, 48 and 36. Thus the magnitude reduction of higher frequencies does not appear in the CWD result to the same large degree as with the WT. Also as can be clearly seen in Fig. 11, the WT results show that the single frequency input signal has intensity that increasingly spreads over a wider frequency range in the WT result as the
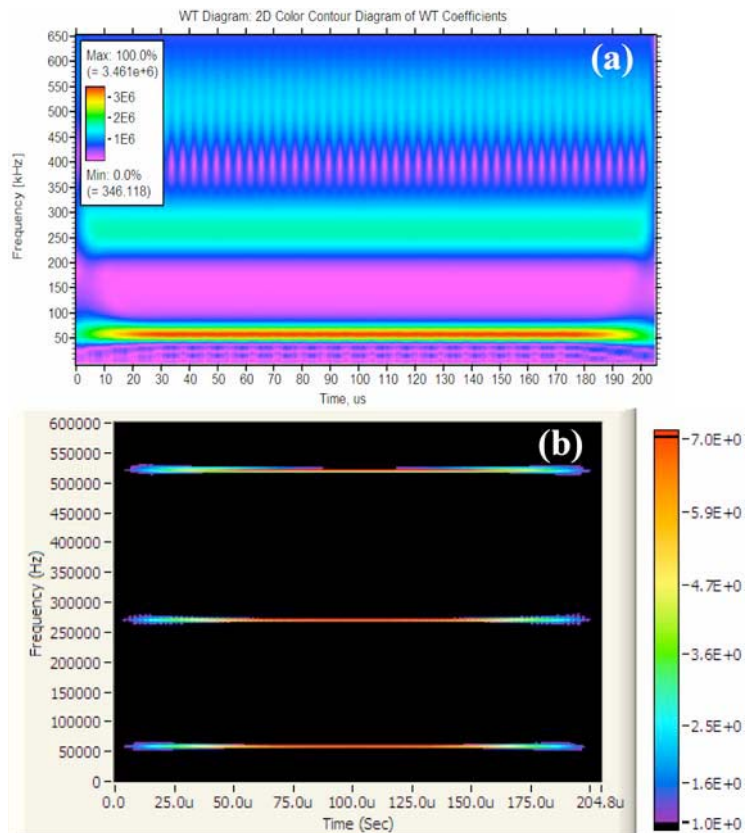
Fig. 11. Results for WT (a) and CWD (b) both applied to signal comprised of superposition of sine waves of equal amplitude at frequencies of 60 kHz, 270 kHz and 522 kHz.
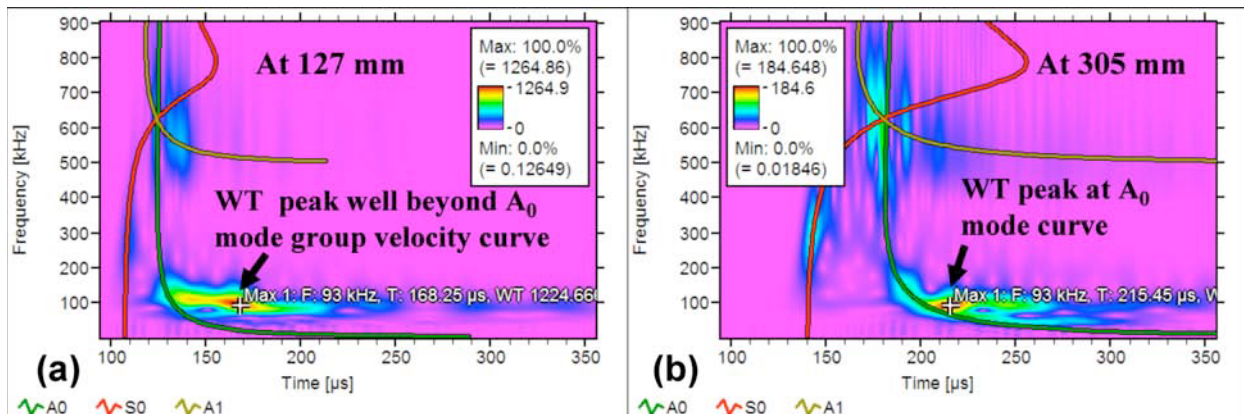

Fig. 12. Illustration of cause of group velocity error with resonant Res #1 sensor at 93 kHz for PLB source near bottom edge. Shows in (a) the peak is not in the same relation to the A_0 group velocity curve as shown in (b).

signal frequency increases. In summary, this contrast between the CWD and the WT results can be expected to result in the CWD frequency of the pair being higher at higher frequency intense modal regions.

The group velocity results in Tables 2 and 3 show that with the wideband sensors, the difference between the experimental velocity and the theoretical values was less than 5 %. For the resonant sensors, the difference between experiment and theory was less than 6.5 %, with one exception. In this case (Res #1 sensor for the near bottom edge source), the most intense region of

the A_0 mode had large differences from the theoretical group velocity (WT – 45 % and CWD – 29 %). Using the WT result, Fig. 12 illustrates the cause of this large difference. This figure shows that at the farther distance the WT peak at 93 kHz was quite close to the A_0 curve, but due to a resonance at the shorter distance, the WT peak was well beyond the A_0 curve even though the intensity began just beyond the A_0 curve. It should be noted that the error with the CWD was still large, but it was considerably less. This result may be due to sharper peaks in time in lower frequency bands with the CWD compared to the WT, as will be demonstrated later in this paper. Such large differences in the experimental versus theoretical group velocities, implies that if arrival times were used from this intense region, poor results would be obtained for calculated source locations.

The results in the tables contribute to a false impression relative to the use of resonant sensors. The reason is that a number of intense regions for these sensors were not included in the table. They were not included due to several facts: (i) the mode associated with the frequency of the intense region changed between the 305 propagation distance and the 127 mm distance; (ii) there was an intensity peak near the intersection of all three modes (at about 625 kHz), and the location of the peak magnitude changed in time relative to this intersection at the two distances; and (iii) the mode of the intense frequency peak could not be determined. These three characteristics were not observed with the wideband sensors. Figures 13 through 15 illustrate some of these aspects with the WT results shown at the two propagation distances. Figure 13 demonstrates a case where the mode corresponding to the peak WT coefficient at a resonant frequency changed when the propagation distance changed. At the 127 mm distance, the peak at 147 kHz was near the A_0 mode. While at the 305 mm distance, the peak was near the S_0 mode. Thus, the signals from the Res #3 sensor at this intense frequency did not provide arrival times at a fixed group velocity for the PLB source near the bottom edge.

Another example with the resonant Res #1 sensor is shown in Fig. 14 for a PLB near the mid-plane. In this case, the WT coefficient peak at 594 kHz changed its relationship in time relative to the intersection of the three modes (A_0, A_1 and S_0) at the two different propagation distances. This change again would yield arrival times from the intense region that did not correspond to a single group velocity at different propagation distances.

A final example to demonstrate the potential issues is shown in Fig. 15. In this case for the Res #1 sensor, the mode of the WT coefficient peak at 573 kHz changed from the A_1 mode at 127 mm to the A_0 mode at 305 mm. This change for a PLB near the bottom edge would not result in peak-determined arrival times at this frequency for the same mode and group velocity when the propagation distance changed. We note that the CWD results were similar for these three examples.

Since the intense mode/frequency combinations generated by AE sources in plates vary as a function of source depth [1] and plate thickness [11], it is not possible to predict ahead of time when a resonant sensor will yield poor results in the determination of accurate arrival times at a particular intense frequency. One resonant sensor (Res #2) yielded accurate group velocity results for the sources at both source depths. This result was likely due to the fact that the intense frequencies were located at points where there was a significant difference in the group velocities of the two fundamental modes, and these frequencies were away from the intersection of all three modes. Thus, the results of the current experiment imply that if one is planning to use time/frequency analysis to obtain accurate mode arrival times, it does not make sense to use resonant sensors unless some significant experimental effort is expended to determine the
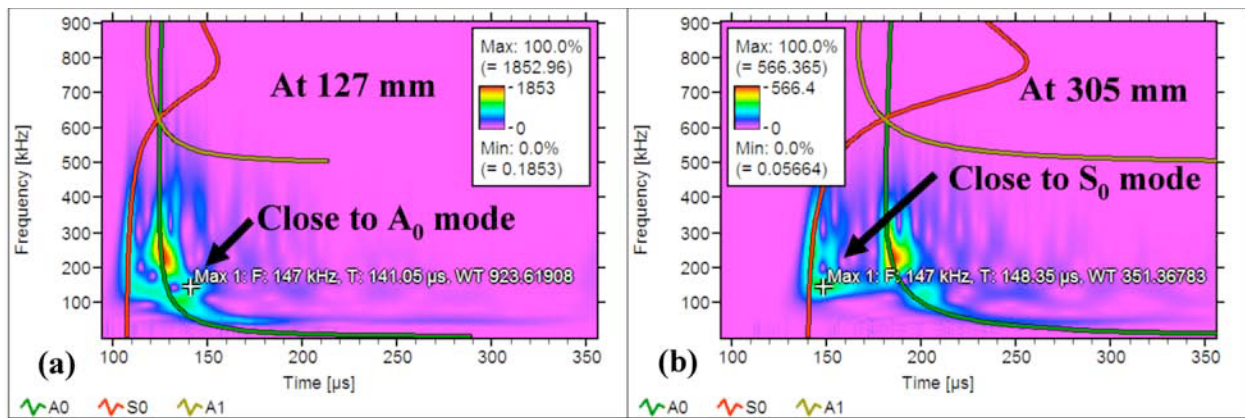
Fig. 13. Example of nearest mode at 147 kHz peak changing with propagation distance for resonant Res #3 sensor for PLB near bottom edge.
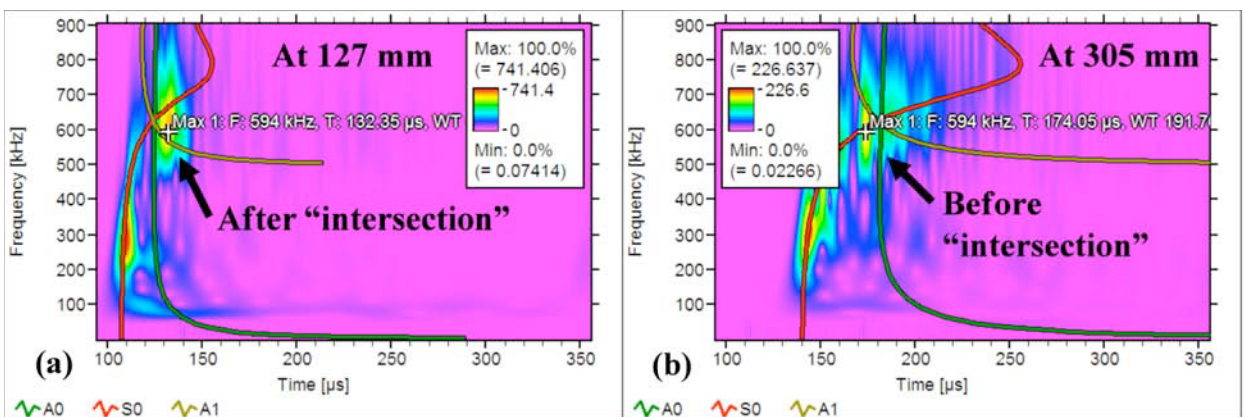

Fig. 14. Example of mode changing relationship in time to intersection of three modes at 594 kHz peak for resonant Res #1 sensor for PLB near mid-plane.
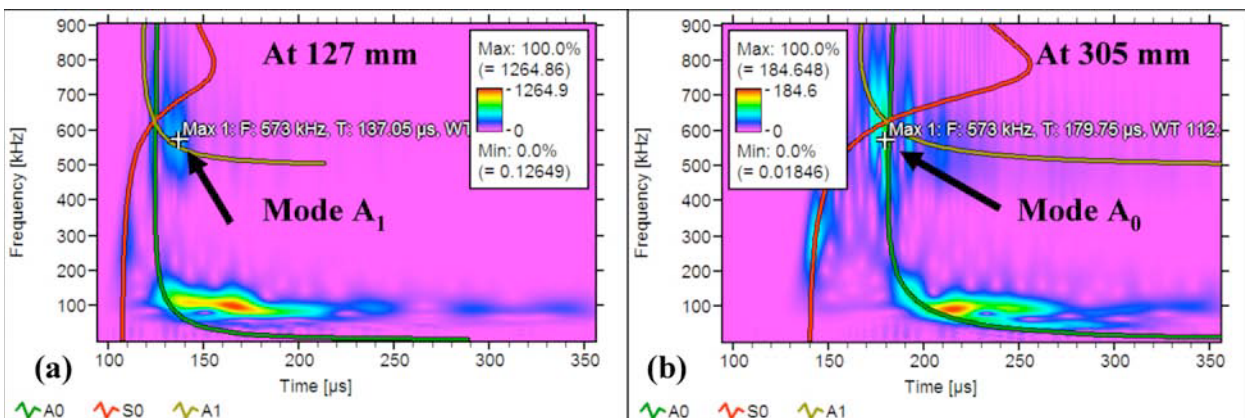

Fig. 15. Example of mode of peak changing with propagation distance at 573 kHz with resonant Res #1 sensor for PLB near bottom edge.

frequencies that should not be used. But, if such effort is invested, then the results from resonant sensors can be used to obtain accurate arrival times that correspond to a single group velocity. Thus, accurate source locations could be calculated by use of resonant sensors with their typical advantage in sensitivity. This situation would enhance AE nondestructive examinations that depend on identifying clusters of events originating from a flaw in a structure that does not have edge reflections (for example a large diameter sphere).

Potential Frequencies for the Sensors for the 3.1 mm Thick Plate

Based on the results in Tables 2 and 3 and the discussion relative to the frequencies that were not included in the table, Table 4 provides potential frequencies (really the high-end frequency of a frequency band) to use with the WT or CWD to obtain accurate arrival times from real AE signals with the different sensors in a 3.1 mm thick aluminum plate. For each sensor, the first line in the table provides a frequency for WT analysis and the second line gives one for CWD analysis. The suggested frequencies are those that were the most intense in the case of the wideband sensors. In the case of the resonant sensors, as can be seen from Tables 2 and 3 the suggested frequencies were not always the most intense for the Res #1 and Res #3 sensors. This table also suggests the frequencies to avoid to prevent obtaining inaccurate arrival times that do not correspond to the same mode arrivals at different propagation distances. Since there are two frequencies (except for one CWD case) associated with each sensor (for the two different depth regions), for real AE testing it will be necessary to select the best frequency for each AE event and to verify that the mode of the peak magnitude arrival time corresponds to the expected one at that frequency. Previous modeling work [14] has shown that the ratio of the peak magnitudes at the two frequencies can be used to choose which frequency will provide the best signal-to-noise ratio. In addition as shown in previous work [15], the group velocities from the two modes at that frequency can be used to verify the mode when source location calculations are made with each group velocity (for the different source depths) using the determined arrival times. The velocity that provides the smallest "Lucy" value [15] identifies the mode and results in the most accurate source location. It is interesting to note in Table 4, that the two resonant sensors, which have frequencies to avoid, result in the frequencies from the intense signal region of the WT and CWD being relatively close to each other, whereas, with the wideband sensors, the paired intense frequencies always resulted in the CWD frequency being significantly larger than the WT frequency.

Table 4 Suggested frequencies for arrvial times from the WT and/or CWD.

Sensor	Frequency [kHz], mode for near mid-plane source	Frequency [kHz], mode for near plate surface source	Frequency [kHz] to avoid for near mid-plane source	Frequency [kHz] to avoid for near plate surface source
FHWA	405, A_0	60, A_0	----	----
	463, A_0	61, A_0	----	----
WB #1	351, S_0	60, A_0	----	----
	371, S_0	61, A_0	----	----
WB #2	375, S_0	138, A_0	----	----
	397, S_0	151, A_0	----	----
Res #1	306, S_0	300, S_0	594	93, 573
	307, S_0	----	610	100, 581
Res #2	510, S_0	441, A_0	----	----
	527, S_0	466, A_0	----	----
Res #3	252, S_0	231, A_0	----	147
	251, S_0	239, A_0	----	151

On the Use of the WT and CWD to Determine Arrival Times for Thicker Plates

If one considers the situation for thicker plates where more modes will be present (in the normal frequency range used in AE) and will be in closer proximity in time and frequency, the
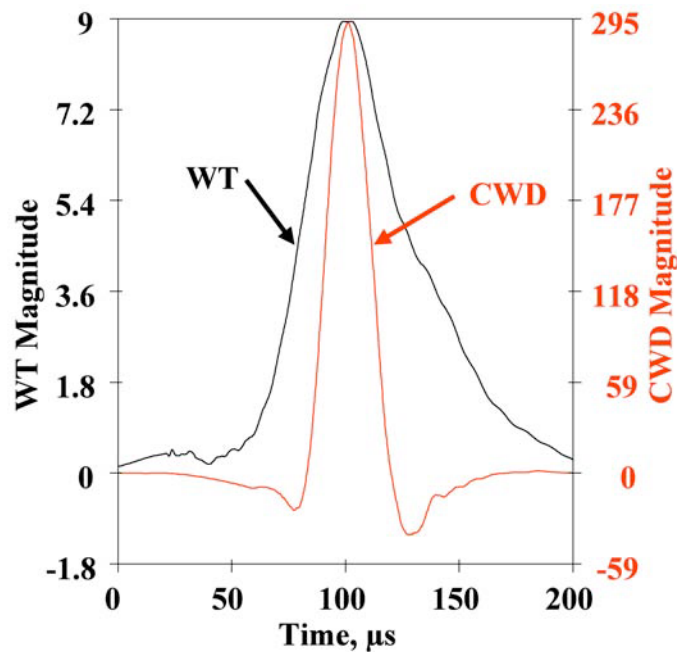
Fig. 16. Magnitude of CWD and WT coefficients versus time for nominal 60 kHz band, FHWA sensor and near bottom edge source for propagation distance of 305 mm.

accuracy of the mode arrival-time results determined with the WT versus those determined with the CWD may be different. In these thicker plates in the typical frequency range for AE monitoring, it may be expected that the CWD will be more likely to provide results not determined by a combination of modes. This result is likely to be due to the sharper peaks of mode arrivals with CWD as a function of time at <u>lower frequencies</u>, as shown in Fig. 16. In this case for a near bottom edge PLB source with the signal from the FHWA sensor, the CWD peak corresponding to the arrival of the A_0 mode is sharper than that from the WT for the same signal. Thus there would be less opportunity for adjacent mode arrivals at this frequency to result in a peak magnitude from more than one mode when the CWD is used.

Further, the potential superiority of the CWD in this plate may be due to sharper peaks at a fixed signal time as a function of frequency at <u>higher frequencies.</u> As an example one can consider the related pair of intense arrivals from a near mid-plane PLB source and the FHWA sensor data at a propagation distance of 305 mm. In this case, the WT magnitudes from the same arrival time at 10 % above and 10 % below the peak frequency of 627 kHz (S_0 mode) were respectively 90 % and 88 % of the peak magnitude at the peak frequency. In contrast, the CWD respective magnitudes from the same arrival time at 10 % above and 10% below the peak frequency of 661 kHz (S_0 mode) were respectively 4 % and 21 % of the peak magnitude at the peak frequency.

Finally, based on the current thin-plate results, it may be expected with resonant sensors that there will be a set of frequencies to avoid in thick plates.

Conclusions

In the case of a relatively thin and large plate:
- Use of either the WT or the CWD allows easy determination of the arrivals of the two fundamental modes with both the resonant and wideband sensors used in this study.

58

- Even though the different sensor models responded to nearly the same waves, there was a wide range of intense frequencies for the signals from PLBs at each of the two source depths.
- The experimental group velocities as determined with all the sensors (with one exception) were close to the theoretical values (less than 6.5 % difference) when certain intense frequencies of the resonant sensors were not used to obtain arrival times and group velocities.
- Cases that were ignored with the resonant sensors primarily dealt with an inability to identify any precise and/or consistent mode arrival at each propagation distance.
- Typically the high intensity regions determined with the CWD occurred at a higher frequency compared with the WT-determined frequencies for each intense modal region. This result is consistent with the fact that at higher frequencies the WT (in contrast to the CWD) spreads the intensity from a single frequency signal into adjacent frequency regions.
- At lower signal frequencies, the CWD magnitude results had sharper peaks (as a function of time) at mode arrivals than the WT. In addition, it also had sharper peaks (as a function of frequency) than the WT at higher frequencies.
- It might be expected that the CWD will provide more accurate arrival time results than the WT for thicker plates when more modes will be present and will be closer in time to each other.

Acknowledgement

References

1. M. A. Hamstad, A. O'Gallagher and J. Gary, J. of Acoustic Emission, **20**, 2002, 39-61.
2. M.A. Hamstad, J. Gary and A. O'Gallagher, J. of Acoustic Emission, **20**, 2002, 62-82.
3. K. S. Downs, M. A. Hamstad and A. O'Gallagher, J. of Acoustic Emission, **21**, 2003, 52-69.
4. M.A. Hamstad, K.S. Downs and A. O'Gallagher, J. of Acoustic Emission, **21**, 2003, 70-94 and A1-A7
5. M. A. Hamstad and A. O'Gallagher, J. of Acoustic Emission, **22**, 1-21, A1-A7, 2004.
6. M.A. Hamstad and A. O'Gallagher, J. of Acoustic Emission, **23**, 2005, 1- 24.
7. M.A. Hamstad, *Advanced Materials Research*, **13-14**, 2006, 61-67.
8. M.A. Hamstad, J. Acoustic Emission, **25,** 2007, 92-106.
9. M.A. Hamstad and C.M. Fortunko, *Nondestructive Evaluation of Aging Bridges and Highways,* Steve Chase, Editor, Proc. SPIE 2456, pp. 281-288, 1995.
10. M.A. Hamstad, Wood and Fiber Science, **29** (3), 1997, 239-248.
11. M. A. Hamstad, J. Gary and A. O'Gallagher, J. of Acoustic Emission, **16**, (1-4), 1998, S251 to S259.
12. Vallen, J., *AGU-Vallen Wavelet transform software* version R2007.0309 and *Vallen Dispersion software* version R2006.1024, Vallen-Systeme GmbH, Icking, Germany (2007).
13. LabVIEW, *Signal Processing Toolkit*, Version 7.5, National Instruments, Austin, TX.
14. M.A. Hamstad, ICAE-6, *Advances in Acoustic Emission*, 2007, pp. 247-252
15. M.A. Hamstad, J. Acoustic Emission, **25,** 2007, 194-214.